Paper presented at Nuclear Science and Nuclear Power Systems Symposium, Orlando, Nov 9-11

TRI-PP-88-94
Nov 1988

DESIGN OF A VOLUME-IMAGING POSITRON EMISSION TOMOGRAPH

J.G. Rogers*, R. Harrop*†, G.H. Coombes*, N.A. Wilkinson*, M.S. Atkins†, B.D. Pate*, K.S. Morrison*, M. Stazyk*, C.J. Dykstra*†, J.S. Barney*†, P.W. Doherty‡ and D.P. Saylor§

*TRIUMF, 4004 Wesbrook Mall, Vancouver, B.C., Canada V6T 2A3
†Simon Fraser University, School of Computing Science, Burnaby, B.C. Canada V5A 1S6
‡Dept. of Nucl. Med., VA Medical Center, West Roxbury, Boston, MA 02132, USA
§Tracergraphics, Inc., 4 Sherburne, Rd., Westboro, MA 01518, USA

Abstract

Progress is reported in several areas of design of a positron volume imaging tomograph. As a means of increasing the volume imaged and the detector packing fraction, a lens system of detector light coupling is considered. A prototype layered scintillator detector demonstrates improved spatial resolution due to a unique Compton rejection capability. The conceptual design of a new mechanism for measuring scattered radiation during emission scans has been tested by Monte Carlo simulation. The problem of how to use effectively the resulting sampled scattered radiation projections is presented and discussed.

Introduction

Positron volume imaging (PVI) [1] instruments have a potential advantage over conventional slice oriented tomographs in that they have a larger geometric efficiency for detecting emitted gamma radiation. A detector suitable for such a PVI instruments has been designed [2] and preliminary results were presented at the conference last year [3]. The useable area of the detector has been enlarged by substituting a 130 mm diameter imaging photomultiplier tube (PMT), the Hamamatsu R3292, for the 75 mm square PMT previously used.

Detector Testing

In tests similar to those reported earlier [3], the new detector demonstrated intrinsic spatial resolution which varied in the range 4-6 mm FWHM over the useable detector area. This area, defined to be the region where the position response is linear, was measured to be approximately circular and 75 mm in diameter. The spatial resolution, measured by scanning a narrow gamma ray beam across the face of the 25 mm thick NaI crystal, varied inversely with the signal size from the imaging PMT to which it was coupled. The first PMT tested contained a region of low pulse height response perhaps due to a defect in the cathode deposition, covering about one-third of the useable diameter. Avoiding this region of low response the spatial resolution was in the range 4-5 mm FWHM. A second R3292 PMT of improved design has undergone preliminary testing and shows uniform pulse height response over the entire useable area.

Increasing the Packing Fraction

Although the useable area of the existing detector is larger than with the previous design [3], 75 mm is still too small for practical volume imaging of either brain or heart. Some means of increasing the useable area is needed. It is also desirable that this area be rectangular rather than circular so that detectors can be mounted close together in a ring tomograph geometry to obtain a large packing fraction. One possible way to increase the useable area and make it rectangular, is to use a lens system to reduce the size of the scintillation light image between its source in the crystal and the PMT cathode. This would allow the use of much large scintillator crystals with the existing 75 mm square or 130 mm diameter round PMT's. A lens system was reported long ago [4] for coupling a thin NaI scintillator to a 50 mm diameter image intensifier tube. Although that previous system was abandoned because not enough light was transmitted by the lens, our requirements seemed at first to be less demanding on the lens design. We require less demagnification due to our smaller crystal diameter and larger PMT diameter, and in addition we image with 511 keV gammas instead of 140 keV ones, so there are more photons to start with.

A relay lens system was designed by a commercial lens designer [5] to have a magnification of 0.45 and a geometrical light collection efficiency of 1.3% in the NaI. This level of lens performance is about the minimum required to obtain a reasonable field-of-view diameter (75mm/0.45 = 170 mm) and an intrinsic PMT spatial resolution around 2 mm FWHM [6]. The design arrived at consisted of 7 custom lens elements, the largest one being a 40 cm diameter plano-convex collector 26 cm from the entrance window of the NaI. The overall length of the designed lens system was 80 cm. A ring tomograph containing such lenses would be about 3 m in outside diameter. Because of the large size, and because of the cost of custom lens fabrication, this means of increasing the packing fraction was not pursued beyond the theoretical lens design phase.

One alternate means of increasing the packing fraction which is being considered is to use four 75 mm square (Hamamatsu R2487) imaging PMT's to cover a 150 mm square scintillation. This has the advantage of obtaining the desired shape for the useable area, and could be easily extended to larger area detectors. Measurements will be carried out to determine the performance of such a detector, especially for scintillations occurring near the gaps between the square cathodes.

Compton Suppression in Layered Scintillators

The spatial resolution of the detectors can be improved by recognizing and rejecting detected events in which more than one light-producing interaction has occurred in the scintillator. Compton scattering produces such multiple interaction events in NaI (and to a lesser extent in the other scintillators used for PET). Because the scattered gamma ray travels some distance in the crystal between interactions, the scintillation light is randomly spread out and so such events are expected to lead to poorer spatial resolution than single vertex events [2].

One method of correcting for such "Compton broadening" has been tested. A layered scintillator was constructed by Bicron Corporation of Newbury, Ohio. It consisted of four layers of 15 x 15 x 1.25 cm NaI crystals, hand polished and joined into a

single $15 \times 15 \times 5$ cm block with optical cement. As shown in Fig. 1, the crystal was viewed by a 130 mm diameter imaging PMT on a 15 cm square face, and by individual (non-imaging) PMT's on the 15×1.25 cm side-faces of the layers. Due to the lower index of refraction of the optical cement (1.48) compared to NaI (1.85), about 60% of the light emitted in a layer is channeled to the edges of the layers by the process of total internal reflection. A portion of this channeled side-going light is detected by the side-coupled PMT's so that each event is characterized by the distribution of its light among the layers in addition to the usual light distribution on the face of the imaging PMT.

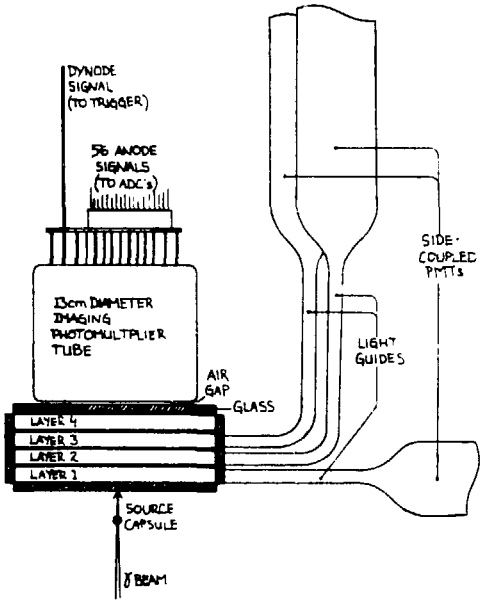

Fig. 1. Apparatus used for testing the layered scintillator

energy in layer-1; region-4 events leave full energy in the crystal but no energy in layer-1; and region-5 events leave full energy in the crystal but less than full energy in region-1. (Although region-3 and region-4 events produce no light in layer-1, some of them are displaced slightly from the horizontal axis in Fig. 2 because of optical cross-talk in the side window, which is common to all four layers.) Of the events that interact (i.e. leave some energy) in layer-1, those in region-5 are multiple vertex and can be rejected. Those in regions-1 and -2 are likely to be single-vertex. We cannot say for sure that they are single vertex, because multiple interaction events may occur inside a single layer. To minimize the probability of multiple interactions, the layers ideally should be thin compared with the gamma interaction length in the crystal (30 mm in NaI at 511 keV) [8].

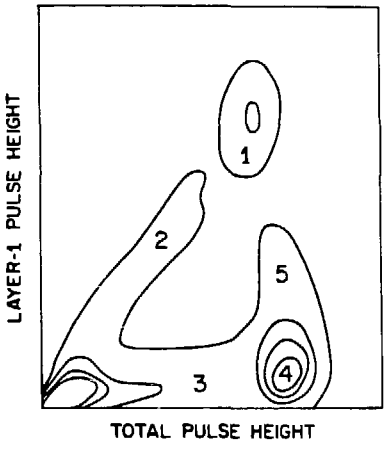

Fig. 2. Contour plot of the number of events as a function of the pulse height in the imaging PMT (horizontal) and the pulse height in the side-coupled PMT attached to layer-1 of the layered scintillator (vertical)

The face coupled (imaging) PMT measures the pulse height for each event summed over all layers because a portion of the light from each scintillation is emitted toward one of the 15 cm square faces and eventually emerges into the imaging PMT, either directly or after reflection from the reflector opposite the imaging PMT. A single-vertex event is characterized by a proportional division of light between the imaging PMT and one of the layers. The proportion is a function of the relative refractive index and light-collecting geometry, but more or less independent of the vertex position in the crystal. Because the angular distribution from Compton scattering of gamma rays is forward peaked [7], most multiple-vertex events can be recognized by a distribution of side-going light among two or more layers. Events having side-going light emission from more than one layer can thus be rejected as multiple-vertex.

Figure 2 shows a contour plot of the number of detected event as a function of the pulse height of the face-coupled PMT and one of the side coupled PMT's, namely that for layer-1 in Fig. 1. Numbered regions correspond to different classes of gamma interactions in the layered crystal, as follows: region-1 events interact only in layer-1 and deposit all their energy in that layer; region-2 events also interact only in layer-1 but they leave less than their full energy in the whole crystal assembly; region-3 events leave less than full energy in the crystal and no

Distributions of events in the other layers are qualitatively similar to, though different in detail from, that shown for layer-1. When multiple-vertex events are eliminated by selecting only single-vertex full energy (region-1) events, the apparent spatial resolution improves. Figure 3 shows the improvement obtained for layer-2 which is typical of that for the other layers. Rejecting the identified multiple vertex events improves the resolution at the FWTM by a large amount but only slightly at the FWHM. However, about half the detected events get rejected by the imposition of this single-vertex requirement. These studies verify that Compton rejection is possible in principle by using layered scintillators.

The configuration tested was by no means optimum. The layers of optical coupling material between the several scintillator layers scatter a substantial amount of light and give the crystal a milky appearance. As a result the spatial resolution was found to be less than optimum in the layered crystal, namely about 20% worse than in the unlayered crystal described earlier. Performance would certainly improve in a layered crystal with a clear (i.e. non-diffusing) optical coupling between the layers. Such coupling material is available as an option from the manufacturer (Bicron) but we did not specify it when the present crystal was ordered.

The side-coupled PMT's also provide an independent mea-

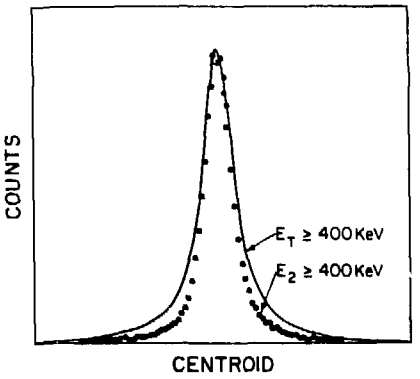

Fig. 3. Typical centroid spectrum without suppression of events from Compton scattering (solid curve) and with such suppression (points)

sure of the depth-of-interaction. Figure 4 shows the spectrum of events as a function of the depth-of-interaction, estimated for each event as the square of the second moment of the light distribution measured by the imaging PMT [3]. In the 'total' spectrum of Fig. 4 events were selected only by requiring the total pulse height measured by the imaging PMT be in the "photopeak" of the energy spectrum. In the two lower curves, events were selected with the additional condition that the light be emitted entirely from within a single layer (such as those in region-1 of Fig. 2) as described above. The figure shows the expected correlation between depth estimated by second moment and depth measured directly by the side-coupled PMT's. The long tail on the right of the 'layer-4' depth spectrum may be due to events with multiple interaction vertices, in which the first vertex corresponds to small angle (small energy loss) scattering. Such events could perhaps be rejected if a narrower pulse-height selection were made on the signal from the layer-4 side coupled PMT (to exclude events which were only slightly below the photopeak pulse height in layer-4); however, this was not possible in the present detector because of the poor light collection efficiency of the side-coupled PMT's, resulting in the poor energy resolution in Fig. 2.

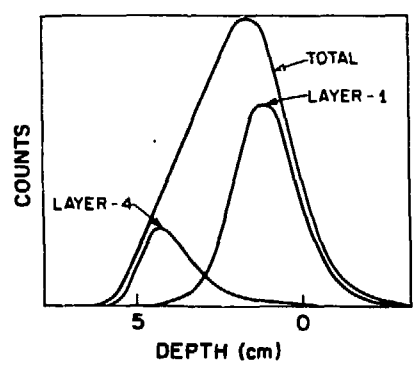

Fig. 4. Number of events as a function of depth estimated by second moment, of the emitted light distribution for all events (total), those interacting in layer-1, and those in layer-4

New Apparatus for Scatter Correction

To supplement the popular software method of scattered radiation correction (by Bergstrom *et al.* [9]), we have developed a concept for a hardware device to measure scattered radiation during PET emission scanning. The apparatus consists of a orbiting pin-sink, which is mechanically similar to the orbiting pin-source used by several groups [10-12] for measuring attenuation. Figure 5 shows how the pin-sink would work. The pin-sink is a cylindrical lead bar thick enough to absorb most 511 keV gamma rays. Its position is recorded with each detected coincidence event. Recorded events may be identified as arising from scattered radiation if the reconstructed coincidence line passes through the position of the pin-sink at the instant the event was recorded. For example, one of the gamma rays detected at points A and B in Fig. 5 must have scattered in the object, perhaps at point C; the coincidence line connecting A and B passes through the (opaque) pin-sink so that unscattered gammas could not have reached points A and B without passing through it. Using this apparatus during an emission scan, detected events with coincidence line passing through the pin-sink can be assembled separately to form a projection of scattered radiation events.

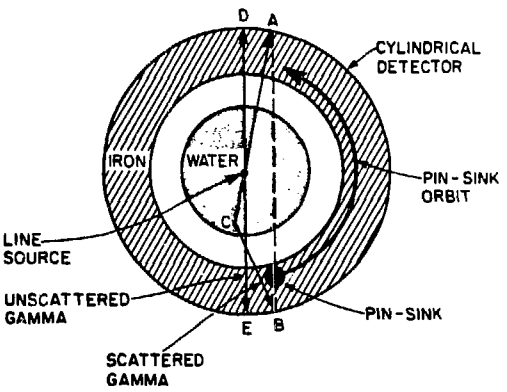

Fig. 5. Conceptual design of a pin-sink apparatus for sampling scattered radiation during PET emission scanning

To see how well the sampled scattered radiation projection resembles the complete scattered radiation distribution, a simulation was performed using Monte Carlo techniques [3]. Only a preliminary study has been completed, with a view toward investigating the possible pitfalls of the method in a rough qualitative sense. The tomograph geometry for simulation was selected to maximize the scattered radiation problem, namely a 42.5 cm diameter cylindrical PVI detector viewing a 20 cm diameter cylindrical water phantom (Fig. 5). A 3 cm diameter lead pin sink was simulated, orbiting between phantom and detector in a 17 cm diameter orbit. Figure 6 shows the scattered radiation distribution from a line source along the central axis of the 20 cm cylinder. The upper curve is a projection formed from the events identified as arising from scattered radiation by their Monte Carlo histories, which we call the 'actual' scattered radiation distribution from the source. The two lower curves (labeled "R-factor") show the ratio of the actual distribution to the distribution of events identified by the orbiting pin-sink for two different sources. The R-factor is the multiplicative factor by which

the pin-sink sampled projection would need to be multiplied, to transform it into the actual distribution. It is a renormalization factor for the pin-sink data which takes into account the distortions in the sample of events from scattered radiation which would be produced by the pin-sink orbiting mechanism geometry. If the shape of the pin-sink sampled projection agreed with the actual distribution, the R-factor curve would be a constant, related to the average solid angle subtended by the pin-sink.

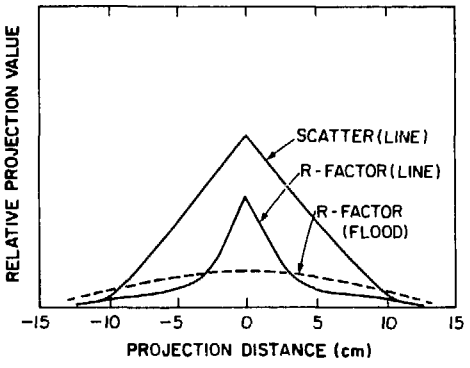

Fig. 6. Simulated scattered radiation projection from a line source in a 20 cm water cylinder (upper solid curve), its ratio to pin-sink identified scattered radiation (lower solid curve), and a similar ratio for a 20 cm flood source (dashed curve)

There are two effects which distort the pin-sink identified distribution from the actual distribution. Near the center of the projection, data from the pin-sink are depressed due to attenuation of small-angle scattered radiation in the pin-sink. Referring to Fig. 5, the scattered radiation events contributing to projection line AB are sampled more efficiently by the pin-sink when point C is far from the line DE than when it is close to it. In other words, the pin-sink sampling mechanism is more sensitive to large angle scattering than small angle scattering, because much of the small angle scattered radiation does not deviate from its original direction by distances large enough to pass the pin-sink without being absorbed by it. The peak in the R-factor occurs at the position of the line source, where the scattering is predominantly small angle scattering. The shape of the R-factor in this region is critically dependent on the diameter of the pin and on the gamma detection energy threshold, but no systematic study of the dependence has yet been undertaken.

The other effect which distorts the R-factor from the desired constant is the sinusoidal variation in the velocity of the pin expressed in terms of the projection distance, which is the absissa of Fig. 6. The component of the orbit velocity along the projection axis is maximum at the centre and zero at the radius of the pin's orbit. Because the pin-sink spends less time at the centre than elsewhere, the "dwell time" effect depresses further the sampling of the central regions of scattered radiation projection by the pin-sink. However the effect varies smoothly inside the object boundary as long as the pin orbit radius is substantially outside the boundary of the scattering object.

The distortion of the scattered radiation distribution by the pin-sink sampling mechanism is different for different source distributions. The dashed curve in Fig. 6 is the correction factor needed to renormalize the sampled scatter of radiation distribution from a 20 cm diameter cylindrical water filled flood source. It is very different from the corresponding factor for the line source (shown in the same figure), even though the scattering medium is the same.

Summary and Conclusions

We have presented progress on research in several areas of the design of positron volume imaging (PVI) tomographs. Area detectors for 511 keV gammas based on the new Hamamatsu R3292 PMT have good resolution, linearity, and depth-of-interaction capability inside a 75 mm diameter central region. However the current design is still too small for use in a practical ring tomograph. As a means of increasing the useable area, a demagnifying lens coupling system was considered but rejected.

Layered scintillators offer a means of correcting for some of the resolution loss due to Compton scattering in large crystal detectors. The improvement is substantial with NaI but would be less for scintillators with higher stopping power.

The conceptual design of an orbiting pin-sink mechanism for separately measuring scattered radiation during emission scans has been presented. Although the idea seems promising, Monte Carlo simulations show that a significant distortion is introduced by the sampling process, and therefore that the sampled projections cannot simply be subtracted from the corresponding emission data. Development of a processing algorithm to utilize the new data in practical scattered radiation correction calculation is needed.

Acknowledgements

We thank W.L. Rogers for providing a list of earlier references on lens coupled gamma camera optics. We acknowledge useful discussions with W.K. Kubler and S. Ziegler on the topic of the pin-sink. This work was supported in part by grants from Simon Fraser University.

References

[1] C.J. Thompson, The Effect of Collimation on Scatter Fraction in Multislice PET, IEEE Trans. NS-35, 598, (1988).

[2] J.G. Rogers, D.P. Saylor, R. Harrop, Yao X.G., C.V.M. Leitao and B.D. Pate, Design of an Efficient Positron Sensitive Gamma Ray Detector for Nuclear Medicine, Phys. Med. Biol., 31, 1061, (1986).

[3] J.G. Rogers, R. Harrop, P.E. Kinahan, N.A. Wilkinson, G.H. Coombes, P.W. Doherty, and D.P. Saylor, Conceptual Design of a Whole Body PET Machine, IEEE Trans. NS-35, 680 (1988).

[4] J.G. Mitchel, J.R. Mallard, I.B. Egerton, A.B. Caldwell, A.V. Lakshmaman, C. Nunan, and W. Turnbull, Towards a Fine-resolution Image-intensifier Gamma-camera, Medical Radioisotope Scintigraphy (Proc. Symp. Monte Carlo, 1972), IAEA, Vienna, 157 (1973).

[5] R.A. Buchroeder, Optical Design Services, 2939 E. 3rd St., Tucson, AZ 85716, Private Communications.

[6] H. Kume, S. Muramatsu, and M. Iida, Positron Sensitive Photomultiplier Tubes for Scintillation Imaging, IEEE Trans. NS-33, 362 (1986).

[7] R.D. Evans, The Atomic Nucleus, McGraw Hill, Toronto, 691, (1955).

[8] *ibid* 717.

[9] M. Bergstrom, L. Eriksson, C. Bohm, G. Blomqvist and J. Litton, Corrections for Scattered Radiation in a Ring Detector Positron Camera by Integral Transformation of the Projections, J. Comput. Assist. Tomogr. 7, 42 (1983).

[10] R.H. Huesman, S.E. Derenzo, J.L. Cahoon, A.B. Geyer, W.W. Moses, D.C. Uber, T. Vuletich, and T.F. Budinger, Orbiting Transmission Source for Positron Tomography, IEEE Trans. NS-35, 735 (1988).

[11] W.K. Kubler, H. Ostertag, H. Hoverath, J. Doll, S. Ziegler, and W.J. Lorentz, Scatter Suppression by Using a Rotating Pin Source in PET Transmission Measurements, IEEE Trans. NS-35, 749 (1988).

[12] N.T. Ranger and C.J. Thompson, Evaluation of a Masked Orbiting Transmission Source (MOTS) for PET Transmission Scans, Phys. Med. Biol. 33, suppl. 1, 102 (1988).